

# Numerical investigation on crack identification using natural frequencies and mode shapes of a drilling riser during deployment and retrieval

Xingkun Zhou<sup>a,b,\*</sup>, Yuqing Sun<sup>a,b</sup>, Menglan Duan<sup>c</sup>, Wenhua Li<sup>a,b,\*\*</sup>

<sup>a</sup> Department of Marine Engineering, Dalian Maritime University, 116026, Dalian, PR China

<sup>b</sup> National Center for International Research of Subsea Engineering Technology and Equipment, Dalian Maritime University, Dalian, China

<sup>c</sup> College of Safety and Ocean Engineering, China University of Petroleum, 102249, Beijing, PR China

## ARTICLE INFO

### Keywords:

Crack identification  
Drilling riser  
Natural frequency  
Modal shape  
Deployment and retrieval

## ABSTRACT

Deployment and retrieval of drilling risers are among the most highly stressed marine operations processes, and allowable imperfections or missed-inspection cracks are likely to expand into limited defects, making crack identification essential during the deployment and retrieval of risers. This study's main objective is to investigate the performances of natural frequencies and modal shapes on crack identification in a drilling riser during installation and retrieval. First, a computation code is programmed to extract the natural frequencies and modal shapes of the intact and cracked risers, and its validity is verified by two numerical methods, i.e., precise integration method and differential transformation method in the literature. Second, the crack-identification ability of natural frequencies versus crack depth and riser-suspension length is studied in detail. An approach using the normalized fourth derivative of modal shapes is developed for crack identification compared with the traditional modal-curvature and modal-curvature difference approaches. Finally, the cracks near the middle span and both ends of the risers are identified, respectively, during the deployment. From the research on crack identification during installation, several conclusions and suggestions are drawn to provide some valuable references for the safety of drilling and production operations.

## 1. Introduction

Marine drilling riser is an important channel that connects the surface platform to the subsea wellhead. It is one of the weakest parts in a drilling device, which is subjected to complex sea loads, e.g., extreme wind and harsh waves and current, because of its long-span and thin-wall characteristics. Because of manufacturing imperfections, corrosion, high loads, low temperature, wearing, fatigue, and other factors, cracks are unavoidably generated and significantly affect the safety of a drilling-riser system (Peter et al., 2005; API-RP-16Q, 2017). If there are no effective methods are available to detect the micro or potential cracks, fracture failure or accidents will likely occur when the cracks propagate to a critical depth or length, which can eventually cause significant economic loss and marine pollution. On the other hand, when the cracks can be detected in time during the initial process, i.e., deployment, the safety and reliability of the riser system can be ensured, and direct success and the economics of the whole drilling project will be benefited (Wang et al., 2015).

In recent decades, structural damages arising from corrosion, wear, and crack detection on marine risers have been widely reported in the literature. Peter et al. (2005) mentioned that deployment and retrieval were more crucial for the safety of drilling risers in harsh environments and that MP was more sensitive to small cracks than the other traditional NDT methods such as UT, RT, LP, DP, EC, and VM. Further, a 90% detection confidence could only be achieved when the depth of the defect reached 3 mm (Peter et al., 2005; API-RP-14E, 2017). API-RP-16Q (2017) specified that surface cracks were critical and grew the fastest in the region of couplings under high-stress concentrations and in welds. It illustrated that the internal inspection or implementation of a suitable VM applied from the outside was required and that the traditional methods could prove inadequate for deepwater drilling risers because of more complex factor contribution (Peter et al., 2005). Inspection techniques for riser integrity management were summarized in the standard DNV-RP-F204 (2010). However, all of the specified techniques required the riser to be pulled to surface and buoyancy blocks removed, causing difficult, dangerous, and time-consuming operations. Neidhardt et al. (2017) researched UT for wall thickness and crack detection, and

\* Corresponding author. Department of Marine Engineering, Dalian Maritime University, 116026, Dalian, PR China.

\*\* Corresponding author. National Center for International Research of Subsea Engineering Technology and Equipment, Dalian Maritime University, Dalian, China.

E-mail addresses: [zhouxk@dlnu.edu.cn](mailto:zhouxk@dlnu.edu.cn) (X. Zhou), [sunyq@dlnu.edu.cn](mailto:sunyq@dlnu.edu.cn) (Y. Sun), [lwh992@dlnu.edu.cn](mailto:lwh992@dlnu.edu.cn) (W. Li).

### Abbreviations

BOPs	Blowout Preventers
DTM	Differential Transformation Method
DP	Dye Penetrant
EC	Eddy Current
LFJ	Lower Flex/Ball Joint
LMRP	Lower Marine Riser Package
LP	Liquid Penetration
MP	Magnetic Particle
NDT	Non-Destructive Testing
PIM	Precise Integration Method
RT	Radiographic Testing
SPC	Self Programed Code
TLP	Tension Leg Platform
UFJ	Upper Flex/Ball Joint
UT	Ultrasonic Testing
VM	Volumetric Method

concluded that the minimum size for crack detection was 20-mm long and 1-mm deep with an accuracy probability of 90%. Cummins and Todd (2000) discussed an approach for riser inspection and pointed out that the necessary input initial-defect size of the approach was 0.25-mm deep and 20-mm long. API-SPEC-5B (2008) specified that imperfection was allowed as long as the depth was not more than 12.5% of the wall thickness. For top riser joints in a splash zone, Lozev et al. (2003) demonstrated that consistent wetting and drying usually contributed to severe defects and that internal inspections might miss serious defects that could eventually lead to failure (Drummond et al., 2018; Jacques et al., 2010). Tada and Uchida (2012s) modeled a semi-elliptical crack on a pipe section's inner and outer surfaces and evaluated the crack using the direct-current potential-difference method. Min. et al. (2013) assessed the damage, which was considered a decrease in Young's modulus, of a deepwater riser using intact modal information. Liu et al. (2014) analyzed the damage localization and degree of a top-tensioned riser using the autoregressive moving-average model where the damage was seen as a typical reduction in the element stiffness. Huang and Nagarajaiah (2014) investigated a multiple-cracked drilling riser by comparing it with an intact one using a time-frequency-domain approach. Zhou et al. (2017) studied the structure damage, modeled as a reduction in the bending stiffness, of a drilling riser using the traditional mode curvature technique.

As evidenced in the literature, three main features are drawn as follows:

- 1) structural damage is always simplified as a reduction in the whole stiffness.
- 2) intact information is often required so that the damage can be detected based on the difference between the intact and damaged modal results.
- 3) natural frequencies and modal shapes, e.g., curvature and flexibility, are used for damage assessment.

The first issue indicates that the whole stiffness reduction due to damage cannot accurately reflect the specific geometric or physical features of cracks in engineering applications; thus, studying the direct relation between the damage-specific information and detecting index is necessary. The second issue illustrates that obtaining the intact information of a drilling riser is hard or even impossible in engineering, which leads to the demand of a new effective method that only depends on the damaged information is required. The third issue indicates that the difference in the natural frequencies between the intact and cracked risers may be so inconspicuous that the cracks cannot be detected

because of the extremely low fundamental frequencies of the deepwater risers. Besides, the feasibility of traditional crack-identification methods based on the global modal curvature and flexibility for deepwater drilling risers needs to be reassessed.

Therefore, the first objective of the present study is to develop a specific cracked deepwater drilling riser model to explore the relationship of the cracks and crack-identification index. An open crack without a breathing effect is employed to develop such a specific numerical model, which can be simulated using a rotational spring, as referred to in the literature (Ye et al., 2010; Moradi et al., 2011; Zhou et al., 2018). Because deployment is critical in the conventional drilling operation (Peter et al., 2005), the imperfections and crack defects should be evaluated in detail. Further, new cracks keep on initiating and propagating during operation and should be reevaluated to determine which single riser joint can be reused for the next operation, which leads to another need for crack identification during the retrieval. Because the deployment and retrieval processes are reversed, the succeeding crack identifications are all based on the analysis of the deployment, where a hard hang-off mode is the only one considered mode (API-RP-16Q, 2017).

The remainder of this paper is structured as follows. A brief introduction to the drilling-riser system during the deployment, a numerical model with cracks, and the crack-detection theory are presented in Section 2. A code to extract the natural frequencies and modal shapes and the code verification using two numerical methods in the literature are provided in Section 3. The effects of open surface cracks and the feasibility of the crack-identification methods based on natural frequencies and modal shapes are studied in Section 4. Multiple-cracks in the middle span and the cracks at both ends are detected using the first and higher modal results in detail in Section 5.

## 2. Numerical models and detection theory

### 2.1. Transverse vibration model

A TLP that possesses inherent stability and great application is considered in this study to analyze a drilling riser's mechanical behavior during the deployment process (Tian et al., 2019). Fig. 1 shows that the drilling-riser system consists of TLP, UFJ, tensioner, telescopic joint, drilling-riser joints, LFJ, LMRP/BOPs. During the installation, the drilling-riser joints are usually hung off from the spider of the TLP, which is called the hard hang-off mode (API-RP-16Q, 2017), as shown in Fig. 1 (a). The main vibration loads are gravity, buoyancy, axial tension, forces due to the wind, waves, and current, and inertia forces from the riser itself and the water-added mass.

For proper mathematical modeling of the vibration of a drilling riser, the following assumptions are introduced to describe the riser's motions:

- The riser moves only in the plane of waves and current loading directions, as shown in Fig. 1, where the coordinate origin  $o$  is the suspension point, the  $z$ -axis is along with the water depth, and the  $y$ -axis is parallel to the current.
- The pipe is inextensible, and the tension is time-independent, neglecting the longitudinal vibration.
- Length of the riser  $L$  is much higher than its maximum diameter  $D$ , i. e.,  $L/D \geq 1$ , implying that the Euler-Bernoulli beam theory can be employed by ignoring the shear effects.
- Neglecting the stiffness of flowlines, umbilical cables, and buoyancy blocks, the flexural stiffness of the pipe is only related to its material and geometric parameters.
- The clamped stiffness of the spider is infinity, and the telescopic joint, UFJ, and LFJ have not been deployed or remain locked during deployment (API-RP-16Q, 2017; ABS, 2017).
- The structure exhibits a large deflection but experiences small strain, the material behaves linearly elastic, and the damping is negligible

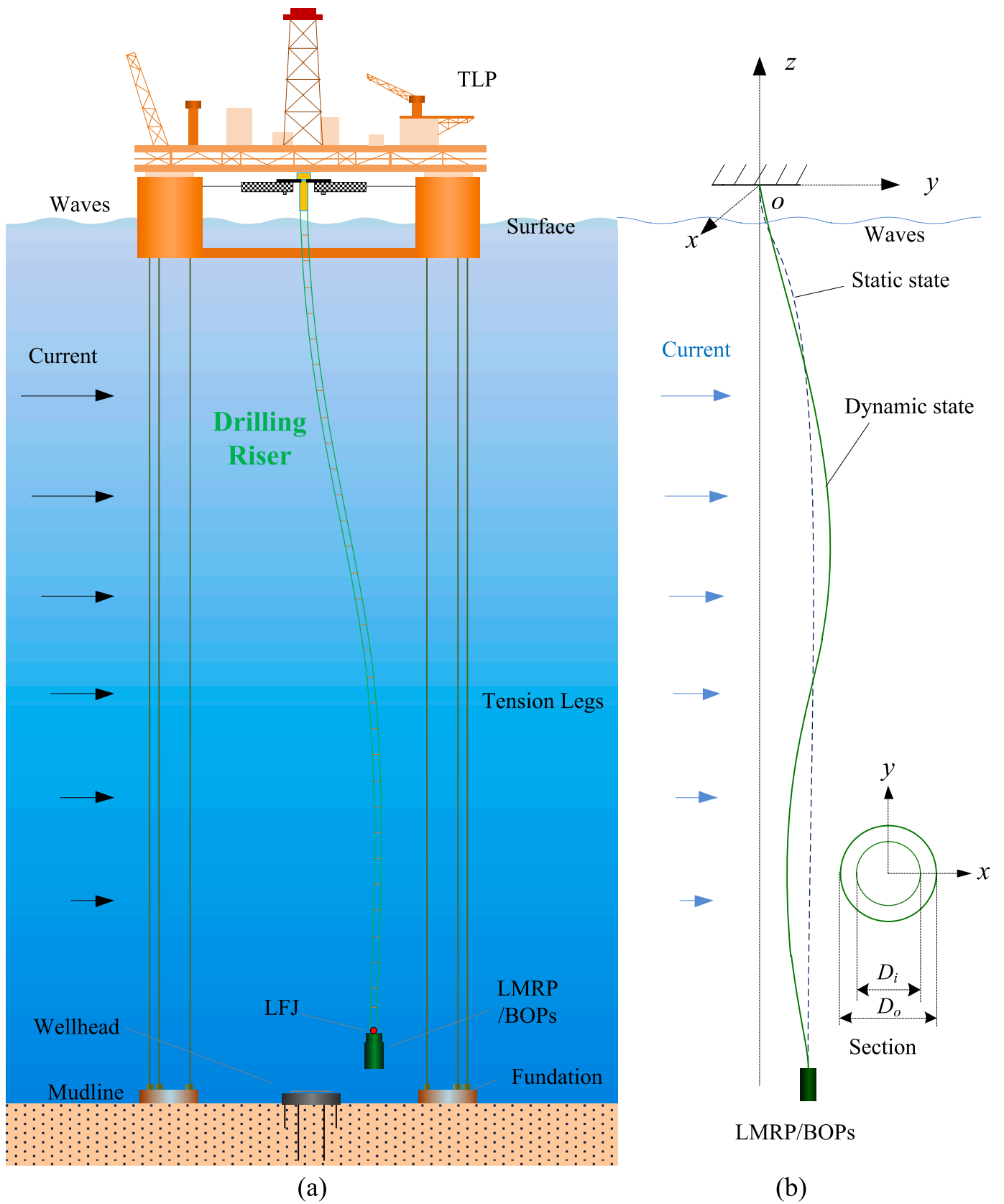


Fig. 1. Schematic of the drilling riser with TLP in the hard hang-off mode.

owing to its small amount compared with the hydrodynamic damping (Lei et al., 2017).

- BOP stiffness is infinite, and its density and cross-section are assumed to be ideally uniform, and the upper end of BOP is considered to be hinged at the lower end of the riser during deployment.

Considering the variable flexural rigidity, axial force, and mass density of a riser, the classical governing equation of free vibration is

$$\frac{\partial^2}{\partial z^2} \left( EI(z) \frac{\partial^2 y}{\partial z^2} \right) - \frac{\partial}{\partial z} \left( T_c(z) \frac{\partial y}{\partial z} \right) + m_c(z) \frac{\partial^2 y}{\partial t^2} = 0 \quad (1)$$

where  $t$  is the time,  $s$ ;  $EI(z)$  is the bending stiffness,  $N.m^2$ ;  $T_c(z)$  is the equivalent axial tension,  $N$ ; and  $m_c(z)$  is the equivalent mass per unit length,  $kg$ ; where

$$T_c(z) = W_B + \int_0^{L-z} w(z) dz \quad (2)$$

and,

$$m_c(z) = \frac{\pi}{4} \rho_r (D_o^2 - D_i^2) + \frac{\pi}{4} \rho_f D_i^2 + \frac{\pi}{4} C_a \rho_w D_o^2 \quad (3)$$

where  $W_B$  is the weight of the LMRP/BOPs,  $N$ ;  $w(z)$  is the apparent weight including the dead-weight and buoyancy per unit length,  $N/m$ ;  $L$  is the total length of the suspension length,  $m$ ;  $D_o$  and  $D_i$  are the outside and inside diameters of the riser respectively,  $m$ ;  $\rho_r$ ,  $\rho_f$  and  $\rho_w$  are the mass densities of the riser, internal fluid, and seawater, respectively,  $kg/m^3$ ; and  $C_a$  is the dimensionless coefficient of the added mass.

Given the boundary conditions, the top end of the hard hang-off riser is usually simplified as a fixed constraint, where the displacement and slope are equal to zero based on the common assumption of the static state of the drilling platform during the deployment, as referred from the literature (Fossum, 2013; Fan et al., 2016; Sheng et al., 2016; Chang et al., 2019; Mao et al., 2019). Hence, the top boundary condition is expressed as

$$y(z, t)|_{z=0} = 0, \quad \left. \frac{\partial y(z, t)}{\partial z} \right|_{z=0} = 0 \quad (4)$$

As a result of LFJ being kept slick during installation (Hariharan and Thethi, 2007), the riser's bottom end can be seen as a free end though there is a massive moment of inertia in LMRP/BOPs (Fossum, 2013; ABS, 2017). Therefore, the riser can be decoupled from LMRP/BOPs beneath LFJ for the modal analysis (ABS, 2017; API-RP-16Q, 2017; Mao et al., 2019; Tian et al., 2019). As expressed in Eq. 5 (a), the moment at the end of the riser is equal to 0. The first two items in Eq. (5.b) represent the forces that arise from the shear force of the riser itself and the LMRP/BOPs tension, respectively, and the third item is the inertia force resulting from the massive mass of LMRP/BOPs (Zhou et al., 2018; Chen et al., 2009). In other words, the bottom boundary condition is

$$EI(z) \frac{\partial^2 y}{\partial z^2} \Big|_{z=L} = 0 \quad (5.a)$$

$$\frac{\partial}{\partial z} \left( EI(z) \frac{\partial^2 y}{\partial z^2} \right) \Big|_{z=L} - T_B \frac{\partial y}{\partial z} \Big|_{z=L} + m_B \omega^2 y(z, t) \Big|_{z=L} = 0 \quad (5.b)$$

where  $T_B$  is the tension at the top end of LMRP,  $N$ ;  $m_B$  is the LMRP/BOPs mass,  $kg$ .

Because the riser behaves linearly elastic, the time-varying shape of the riser can be expressed as a series of eigenfunctions (Dareing and Huang, 1979; Lei and Kaasen, 2006; Yu et al., 2017)

$$y(z, t) = \sum_{j=1}^{\infty} Q_j(t) \psi_j(z) \quad (6)$$

where  $j$  is the modal order,  $\psi_j(z)$  is the  $j$ th order mode shape, and  $Q_j(t)$  is

the  $j$ th order mode weight.

Substituting into Eq. (6) into Eq. (1) gives

$$\sum_{j=1}^{\infty} m_c(z) \psi_j(z) \frac{d^2 Q_j(t)}{dt^2} + \sum_{j=1}^{\infty} Q_j(t) \left[ \frac{d^2}{dz^2} \left( EI(z) \frac{d^2 \psi_j(z)}{dz^2} \right) - \frac{d}{dz} \left( T_c(z) \frac{d \psi_j(z)}{dz} \right) \right] = 0 \quad (7)$$

The summation symbol  $\sum_{j=1}^{\infty}$  and modal order  $j$  are eliminated for the convenience of the following derivation and writing. Letting

$$\omega^2 = \left[ \frac{d^2}{dz^2} \left( EI(z) \frac{d^2 \psi(z)}{dz^2} \right) - \frac{d}{dz} \left( T_c(z) \frac{d \psi(z)}{dz} \right) \right] / [m_c(z) \psi(z)] \quad (8)$$

where  $\omega$  is called as the eigenvalue of the mode weight  $Q_j(t)$ . Eq. (1) is thus simplified as

$$\frac{d^2 Q(t)}{dt^2} + \omega^2 Q(t) = 0 \quad (9)$$

Herein, the eigenvalue  $\omega$  is the key to solve the vibration governing equation Eq. (1). To calculate Eq. (8), the riser's length is divided into  $n$  segments with nodes placed at equal distance  $h$ , as shown in Fig. 2.

Based on the central difference method, the derivatives of mode shape  $\psi(z)$  are.

$$\begin{aligned} \psi' &= \frac{\psi_{i+1} - \psi_{i-1}}{2h} \\ \psi'' &= \frac{\psi_{i+1} - 2\psi_i + \psi_{i-1}}{h^2} \\ \psi''' &= \frac{\psi_{i+2} - 3\psi_{i+1} + 3\psi_i - \psi_{i-1}}{h^3} \\ \psi^{(4)} &= \frac{\psi_{i+2} - 4\psi_{i+1} + 6\psi_i - 4\psi_{i-1} + \psi_{i-2}}{h^4} \end{aligned} \quad (10)$$

where  $\psi'$ ,  $\psi''$ ,  $\psi'''$ , and  $\psi^{(4)}$  are the first, second, third, and fourth derivative  $z$  of  $\psi$ .

Substituting Eq. (10) into the governing equation Eq. (8) and boundary conditions Eqs. (4)-(5), the iterative formula of mode shapes is expressed as

$$\psi_{i+2} + a_i \psi_{i+1} + b_i \psi_i + c_i \psi_{i-1} + \psi_{i-2} = 0 \quad (0 \leq i \leq n) \quad (11)$$

where, the iterative coefficients are

$$\begin{cases} a_i = -4 - \frac{T_i h^2}{EI_i} + \frac{w_i h^3}{2EI_i} \\ b_i = 6 + \frac{2T_i h^2}{EI_i} - \frac{m_c \omega^2 h^4}{EI_i} \\ c_i = -4 - \frac{T_i h^2}{EI_i} - \frac{w_i h^3}{2EI_i} \\ d_i = 1 \end{cases} \quad (12)$$

where  $w_i$  and  $T_i$  are the apparent weight and tension, respectively, at the  $i$ th segment,  $N/m$  and  $N$ .

The boundary conditions become

$$\begin{cases} \psi_0 = 0 \\ \psi_1 - \psi_{-1} = 0 \\ \psi_{n+1} - 2\psi_n + \psi_{n-1} = 0 \\ \psi_{n+2} - (3 + \alpha_T) \psi_{n+1} + (3 + \alpha_m) \psi_n - (1 - \alpha_T) \psi_{n-1} = 0 \end{cases} \quad (13)$$

where,

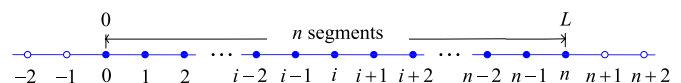


Fig. 2. Divided segments and nodes along the riser.

$$\alpha_T = \frac{T_B h^2}{2EI_n}, \quad \alpha_m = \frac{m_B \omega^2 h^3}{EI_n} \quad (14)$$

Seen from Eqs. (11) and (12), there are  $(n+5)$  equations, which can be written as the matrix form

$$\mathbf{D}\mathbf{Y} = \mathbf{0} \quad (15)$$

where  $\mathbf{Y} = [\psi_{-2}, \psi_{-1}, \psi_0, \dots, \psi_n, \psi_{n+1}, \psi_{n+2}]^T$  is the modal displacement at each discrete node, and  $\mathbf{D}$  is the coefficient matrix related to  $a_i, b_i, c_i, d_i, \alpha_j, \alpha_T, \alpha_m,$  and  $\omega$ . Obviously, there is only one unknown parameter  $\omega$  in  $\mathbf{D}$ .

For free vibration of the drilling riser, the determinant of  $\mathbf{D}$  is zero  $\det|\mathbf{D}| = 0$  (16)

The secant method is utilized to solve the highly sophisticated Eq. (16). After obtaining the natural frequencies, the modal displacements can be obtained via the recalculation of Eq. (15).

### 2.2. Surface open-crack model

When a member is cracked, the strain energy is concentrated around the crack, causing a change in the local flexibility. A specific rotational spring is usually used to quantify the relationship between the strain-energy concentration and loads (Zheng and Fan, 2003; Labib et al., 2014; Yashar et al., 2018). Fig. 3 (a) shows a sketch of the cracked single-riser joint with an open surface crack. For facilitating the analysis, the riser is assumed to be free from fracture and instability despite the crack depth. Fig. 3 (b) shows the cracked cross-section of A-A of the surface open crack, as shown in Fig. 3 (a). Fig. 4 shows that a rotational spring with specific stiffness is employed to simulate the riser section with an open crack.

According to the theory of stress intensity factor in fracture mechanics (Zheng and Fan, 2003; He et al., 2009), the relative rotation  $\theta$  of the cracked section A-A is expressed as

$$\theta = \frac{\partial}{\partial M} \left[ \int_{A_c} G dA_c \right] = \frac{\partial}{\partial M} \left[ \int_{A_c} \frac{K_I^2}{E} dA_c \right] \quad (17)$$

where  $M$  is a moment loading on the member;  $A_c$  is the area of the surface open crack;  $G$  is a measure of the energy-release rate; and  $K_I$  is the stress intensity factor in the near region of a crack tip, which can be expressed as

$$K_I = \frac{M h'}{2I_0} \sqrt{\pi \xi'} F(x_c) \quad (18)$$

where  $I_0$  is the second moment of the uncracked sectional area;  $\xi'$  and  $h'$

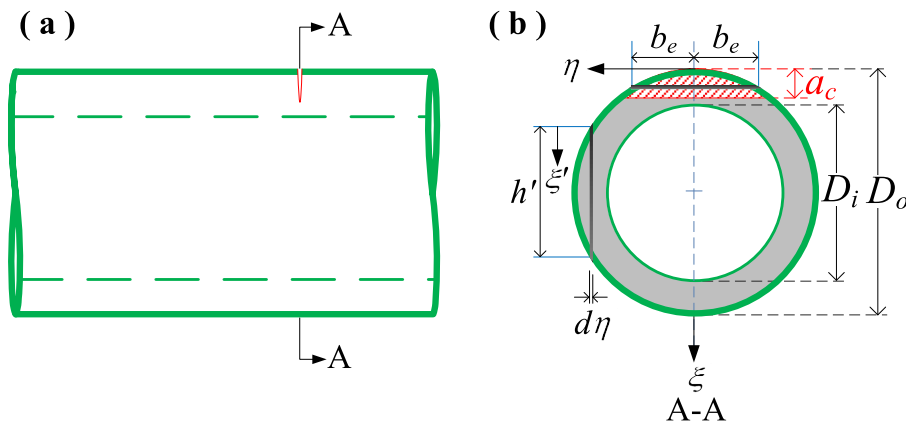


Fig. 3. Cracked riser section a surface open crack.

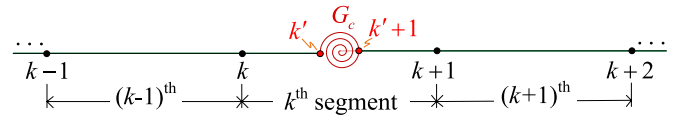


Fig. 4. Equivalent cracked model of a rotational spring with certain stiffness.

are the local coordinates, as shown in Fig. 3(b), which have a geometric relationship with the global coordinates  $\xi$  and  $\eta$ , i.e.,  $\xi' = \xi + \sqrt{D_o^2/4 - \eta^2} - D_o/2$  and  $h' = \sqrt{D_o^2 - 4\eta^2}$ ;  $x_c = \xi'/h'$ ; and  $F(x_c)$  is a function of the local relative position  $x_c$

$$F(x_c) = \frac{\sqrt{\pi x_c / 2 \tan \pi x_c / 2} \left[ 0.923 + 0.199(1 - \sin \pi x_c / 2)^4 \right]}{\cos \pi x_c / 2} \quad (19)$$

Substituting Eqs. (19) and (18) into Eq. (17), the local flexibility coefficient  $C$  (Zheng and Fan, 2003) of the cracked riser section can be obtained

$$C = \frac{\partial \theta}{\partial M} = \frac{1024}{\pi E D_o^3 (1-\gamma^4)^2} \times \int_0^{\frac{\pi}{2}} \left[ \int_{-\sqrt{x_c-x_c^2}}^{\sqrt{x_c-x_c^2}} (1-4y_c^2)(2x_c + \sqrt{1-4y_c^2} - 1) F^2 dy_c \right] dx_c \quad (20)$$

where  $\gamma = D_i/D_o$  and  $y_c = \eta/D_o$ .

Therefore, the equivalent-spring rotational stiffness  $G_c$  of a pipe section with a shallow surface-open crack, i.e.,  $[0 < a_c < (D_o - D_i)/2]$ , in a drilling riser is finally acquired.

$$G_c = 1/C \quad (21)$$

By employing discretization of the drilling riser, and assuming that the rotational spring is located at the middle of one segment, as shown in Fig. 4, the displacements and forces at both sides of the crack are expressed as

$$\begin{cases} y_{k'+1} = y_{k'} \\ \theta_{k'+1} = \theta_{k'} + M_{k'}/G_c \\ M_{k'+1} = M_{k'} \\ S_{k'+1} = S_{k'} \end{cases} \quad (22)$$

where  $\theta, M,$  and  $S$  are the modal slope, bending moment, and shear. We especially note that the continuity of the modal displacement  $y,$  slope  $\theta,$  moment  $M$  and shear  $S$  in Eq. (22) results from the assumption of the crack's existence with negligible thickness in the axial direction of the riser, which means that the positions of the two points,  $k'$  and  $k'+1,$  are coincident in the computation.

### 2.3. Crack-identification methods

As previously mentioned, the existence of a crack causes a change in the rotational stiffness resulting in the shift in the natural frequencies and change in the modal shapes. Conversely, when the difference in the natural frequencies and modal shapes between the intact and cracked structures is tested, the crack parameters, e.g., crack position and severity, are easily determined according to the theory of vibration-based NDT. However, for the drilling-riser system, the natural frequencies and modal shapes differ from those in universal beams obtained from simplified aircraft parts, concrete-filled bridges, or even offshore platform trusses because of the sizeable water-depth span and long-thin features. Therefore, investigating the effect of surface cracks on the natural frequencies and modal shapes of the drilling riser is essential.

During installation, the natural frequencies are significantly reduced because of the significant increase in the riser's suspension length. To assess the effect of the surface open cracks on the natural frequencies, distinguishing coefficient  $p_\omega$  is defined to measure the distinguishability of the natural frequencies between the intact and cracked drilling risers.

$$p_\omega = d\omega / \omega^i \times 100\% \quad (23)$$

where  $d\omega = \omega^i - \omega^c$  is the difference between the intact natural frequency, denoted as  $\omega^i$ , and the cracked natural frequency, denoted as  $\omega^c$ .

As a result of the modal shapes' sensitivity, i.e., the modal displacement and slope, the second-order derivative is often used to detect the structural damage of the drilling riser. According to the central difference method, the formula for the second derivative of modal shape  $\kappa$  is expressed as

$$\kappa_{j,i} = \frac{\psi_{j+1,i} - 2\psi_{j,i} + \psi_{j-1,i}}{(\Delta l)^2} \quad (24)$$

Where subscripts  $j$  and  $i$  indicate the  $i$ th mode and  $j$ th node, respectively, and  $\Delta l$  is the distance between two adjacent nodes.

The normalized second derivative of the modal shape is expressed as

$$\bar{\kappa} = \frac{\kappa}{\max(|\kappa|)} \quad (25)$$

The normalized difference between  $\bar{\kappa}$  of the intact and cracked risers is denoted as

$$\Delta\bar{\kappa} = \frac{\Delta\kappa}{\max(|\Delta\kappa|)} \quad (26)$$

where  $\Delta\kappa = \kappa^i - \kappa^d$ ,  $\kappa^i$  and  $\kappa^d$  are the second derivative of the modal shapes between the intact and cracked risers.

Accordingly, the fourth derivative of the modal shape is derived as follows:

$$l_{j,i} = \frac{\psi_{j+2,i} - 4\psi_{j+1,i} + 6\psi_{j,i} - 4\psi_{j-1,i} + \psi_{j-2,i}}{(\Delta l)^4} \quad (27)$$

The normalized fourth derivative of the modal shape is expressed as

$$\bar{l} = \frac{l}{\max(|l|)} \quad (28)$$

### 2.4. Flowchart and parameters

A computation code, named as *SPC*, is programmed based on Eqs. (1)-(20) using the Matlab package to obtain the natural frequencies and modal shapes of the drilling risers for later crack identification during the deployment. The model developed using the *SPC* is shown in Appendix B. Besides, the total number of the single riser joints is marked as  $n_t$ , and the number of single riser joints that are being installed is denoted as  $n_k$ . When  $n_k < n_t$ , the installation operation is not yet completed. Fig. 5 shows a sketch of the deployment.

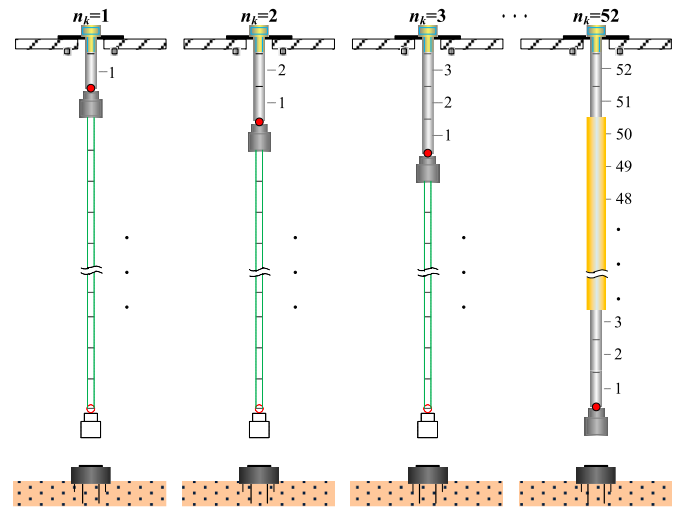


Fig. 5. Schematic of the drilling riser during deployment.

Fig. 6 shows the flowchart of the *SPC* for crack identification during the deployment. The basic computation parameters are listed in Table 1. Where it should be noted that the bottom of the riser should be ensured to keep open to the sea during deployment (API-RP-2RD, 1998; API-RP-16Q, 2017).

Besides, the buoyancy block parameters are considered, and the main properties of the single riser joint with buoyancy blocks are listed in Table 2.

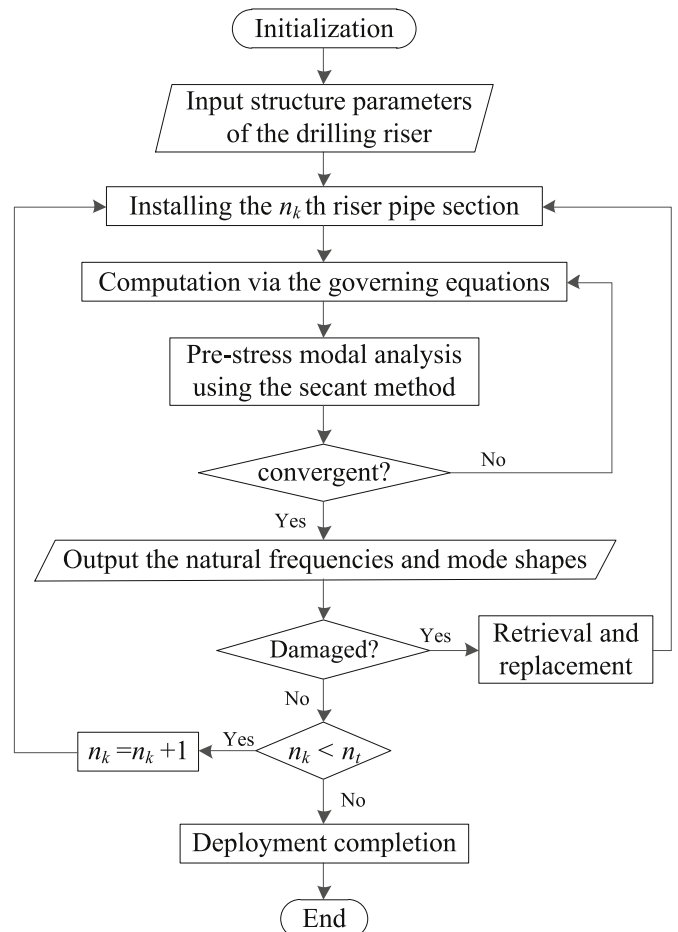


Fig. 6. Flowchart of *SPC* for crack identification.

**Table 1**  
Main properties of the riser system.

Parameters	Value
Water depth $H_w$	1200 m
Single riser pipe section length $l$	22.86 m
Outside diameter of riser $D_o$	0.4730 m
Inside diameter of riser $D_i$	0.4146 m
Steel tube material $\rho_s$	7850 kg/m <sup>3</sup>
Young's modulus $E$	206 GPa
Poisson's ratio $\mu$	0.3
Internal fluid density $\rho_f$	1030 kg/m <sup>3</sup>
Seawater density $\rho_w$	1030 kg/m <sup>3</sup>
Coefficient of added mass $C_a$	1.0
Total mass of LMRP/BOPs $m_B$	200 t
Wet weight of LMRP/BOPs $W_B$	1962 kN

**Table 2**  
Main properties of the buoyancy block.

Parameters	Value
Length of buoyancy block on single riser $L_b$	12 m
Outside diameter of buoyancy block $D_b$	0.945 m
Density of the buoyancy block $\rho_b$	456 kg/m <sup>3</sup>

### 3. Verification

#### 3.1. Intact riser and the riser with different crack locations

Two different methods, namely, PIM (Zhou et al., 2018) and DTM (Chen et al., 2009), are employed to verify the validation of the developed SPC code. We assumed that the suspension length apart from LMRP/BOPs is 114.3 m, which means that five riser joints are hung off, i.e.,  $n_k = 5$ .

Taking the North Sea as an example, the periods of dominant wave components are around 10–12 s while the first two order natural periods of free vibration of the deepwater riser are about 20.3 s and 2.4 s. Higher natural periods get even smaller with the increase of modes. Therefore, very few fundamental natural modes participate predominantly in the vibration of marine risers, and only the first two natural modes can give good convergence to the desired deflection in engineering (Dareing and Huang, 1979; Fossum, 2013). For more accuracy, the first four natural modes are utilized for crack identification of the deepwater drilling riser in this study.

By considering the intact riser and the riser with different crack locations, the first four orders of natural frequencies and modal shapes are obtained to verify the SPC code. As shown in Table 3 and Fig. 7, the results obtained by SPC are consistent with those obtained via PIM and DTM. The preliminary calculation indicates that there is only a minor difference in natural frequencies between the intact riser and the riser with different crack positions.

Note:  $\omega_1$ ,  $\omega_2$ ,  $\omega_3$ , and  $\omega_4$  are the first four orders of natural frequencies, rad/s; subscript  $i$  represents intact riser; and subscripts  $top$  and  $mid$  represent the riser with the top and middle cracks, i.e.,  $l_c = -11.43$  m and  $-57.15$  m, respectively, while the crack depth  $a_c$  is 10 mm.

**Table 3**  
First four natural frequencies of the intact risers.

	$\omega_1$	$\omega_2$	$\omega_3$	$\omega_4$
DTM <sub>i</sub>	0.31004528	2.57711661	5.59254343	9.45108890
SPC <sub>i</sub>	0.31003585	2.57688545	5.59136987	9.44677479
PIM <sub>i</sub>	0.31004528	2.57711661	5.59254343	9.45108822
SPC <sub>top</sub>	0.31003585	2.57688452	5.59135061	9.44668151
PIM <sub>top</sub>	0.31003585	2.57687916	5.59136680	9.44666407
SPC <sub>mid</sub>	0.31004531	2.57711322	5.59251678	9.45100897
PIM <sub>mid</sub>	0.31004538	2.57708543	5.59253903	9.45098752

#### 3.2. The riser with different crack depths

By considering the same model presented in Section 3.1.(a) as an example, the different crack depths are assumed as 5, 10, 15, and 20 mm in the risers. The crack is in the middle of the top second riser joint (i.e.,  $l_c = -34.29$  m). Because of the drawback of the fitting of the global shape of DTM, the crack existence can lead to tedious calculation (Chen et al., 2009; Zhou et al., 2018) and difficulty in applying DTM into the cracked risers.

Through PIM and SPC, the first four natural frequencies are extracted and listed in Table 4.

The first four orders of the modal shapes are calculated using PIM and SPC. The results of the 5- and 15-mm deep risers are shown in Fig. 8.

The data in Table 4 and Fig. 8 show the validation of SPC compared with PIM. Besides, we can easily observe that the small surface open cracks have little effect on the natural frequencies and modal shapes.

#### 3.3. The riser with different suspension lengths

To further validate SPC, cracked risers with the same crack depth of 10 mm, the same crack position (i.e.,  $l_c = -34.29$  m) and different suspension riser lengths (e.g., 114.3, 297.18, 514.2 and 1188.72 m, i.e.,  $n_k = 5, 13, 22$  and 52, respectively) are analyzed when the moment of inertia of LMRP/BOPs is considered.

Through PIM and SPC, the first four natural frequencies of the risers with different suspension lengths are listed in Table 5.

The first four modal displacements of the risers with different hang-off lengths are shown in Fig. 9. The results in Table 5 and Fig. 9 present the validation of SPC compared with PIM when different suspension lengths of the cracked risers are considered. Where “non” indicates that PIM is invalid when the suspension length is longer than about 300 m.

### 4. Analysis and discussion

#### 4.1. Short suspended riser with cracks

As shown in Table 4, crack depth has little effect on natural frequencies when the crack position is fixed, i.e.,  $l_c = -34.29$  m. However, as a result of the cracks that randomly occur at any position during operation, the cracks on the natural frequencies versus the crack position and depth should be studied in detail. By considering the increase in the suspension length in the deployment, two types of risers with 5 and 52 hang-off joints, i.e.,  $n_k = 2$  and  $n_k = 52$ , described as short and long risers, respectively, are employed to determine the effect of the cracks on the natural frequencies.

The single surface-open crack on the first four natural frequencies versus crack location and depth is shown in Fig. 10.

The first-order natural frequencies are sharply reduced with the crack depth increase when the crack is close to the top hang-off constraint. However, the reduction in higher-order natural frequencies of the riser that is cracked near the bottom end is slightly significant than that of the riser that is cracked near the top end. The first two natural frequencies almost do no change despite the increase in the crack depth when the crack occurs between the riser's top and bottom ends.

#### 4.2. Long suspended riser with cracks

When the suspension length is long, taking the end deployment as an example, the first four natural frequencies versus the crack position and depth are shown in Fig. 11.

Fig. 11 shows that the first four natural frequencies sharply decrease when the crack appears near UFJ. However, when the suspension length is longer than approximately 100 m, the natural frequencies are almost the same regardless of the crack depth and position.

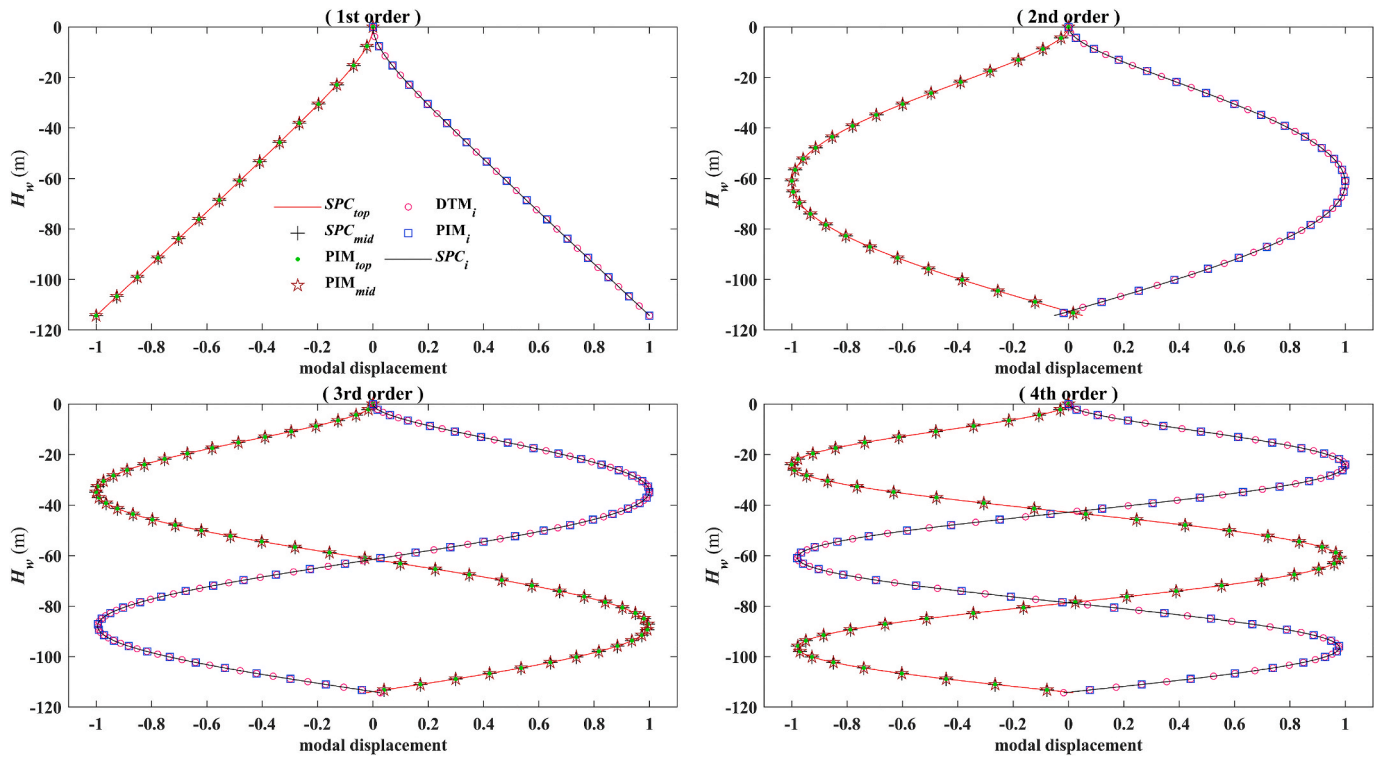


Fig. 7. First four modal shapes of the intact riser and the riser with different crack positions.

Table 4  
First four natural frequencies of the cracked risers with different crack depths.

	$a_c$	$\omega_1$	$\omega_2$	$\omega_3$	$\omega_4$
$SPC_i$	5	0.310035847	2.576885379	5.591367279	9.446770823
	10	0.310035845	2.576884770	5.591355354	9.446754924
	15	0.310035841	2.576883488	5.591330282	9.446721498
	20	0.310035833	2.576881402	5.591289450	9.446667060
$PIM_i$	5	0.310045327	2.577113618	5.592528458	9.451077615
	10	0.310045469	2.577104201	5.592477829	9.451038573
	15	0.310045768	2.577084397	5.592371368	9.450956482
	20	0.310046255	2.577052137	5.592197954	9.450822778

Note:  $a_c$  is the depth of the crack, mm, and  $l_c$  is the location of the crack from the sea surface, m.

### 4.3. Crack detectability of natural frequencies

Marine risers are usually sensitive to a range of resonance phenomena originating from the rig/vessel motions, waves, current and VIV, and the available control-domain excitations are limited to the rig/vessel position and top tension (Fossum, 2013). The specific information of several modes is usually required to assess the crack of a riser. (Zhou et al., 2017; Janeliukstis et al., 2019; Jahangiri et al., 2019). As discussed in Section 3, the natural frequencies almost do not change when the cracks are away from the top end but sharply reduce when the cracks are near the top end, which illustrates the necessity for research on the possibility of crack identification using the fundamental frequencies when the top end is cracked.

When the top end is cracked during the deployment, the variation of the first four orders of natural frequencies versus  $a_c$  and  $L_s$  is shown in Fig. 12. The results in Fig. 12 show that the natural frequencies sharply decrease with the increase in  $L_s$ , the reduction trend of  $\omega_2$  fluctuates when  $L_s$  is less than approximately 200 m, and the natural frequencies remain almost constant with the increase in the crack depth.

Distinguishing coefficient  $p_{\omega}$  based on  $\Delta$  versus  $L_s$  and  $a_c$  is shown in Fig. 13, which are rendered in 3D and 2D views, respectively. The results show that the distinguishable space and area are limited and are mainly

concentrated in the cases of risers with short suspension length and deep crack. For this condition, detecting the open surface cracks is quite difficult or even impossible if the resolution of the employed device is not high. Even if the device resolution can reach 0.05%, the small surface cracks still cannot be detected when  $L_s$  is more than approximately 200 m. In other words, the small difference in the natural frequencies between the intact and cracked risers makes the application of the frequency-based approach impossible for evaluating the shallow (micro) cracks in a deepwater riser.

### 4.4. Crack detectability of modal shapes

Because of the small difference in the natural frequencies between the intact and cracked risers, three methods based on modal displacements and slopes are used to explore the feasibility of crack identification. For convenience in contrast and expression, we consider that five single riser joints are hung off from the TLP in which each riser joint is equally divided into three units, and the cracked numbers are joint-2, joint-3, and joint-4. Besides, the cracks have the same crack depth 0.010 m. Similar to the other cases, the cracks are also located in the middle of the cracked single riser joints. Where subscripts  $v$  and  $\theta$  represent the indexes based on the modal displacement and slope, respectively, the red dashed lines indicate the pre-cracked positions.

Fig. 14 shows that the small cracks cannot be identified by  $\bar{\kappa}$  based on both modal displacement and modal slope. However, when the information of the intact riser is known, the cracks can be accurately identified using  $\Delta\bar{\kappa}$ . When the intact riser's information is unknown, the small open cracks can still be detected using  $\bar{i}$  based on the modal slope.

## 5. Crack identification during deployment

During deployment, the total number of single riser joints is set as 52. From the start to the end of the deployment, as shown in Fig. 5, the value of  $n_k$  changes from 1 to 52. The normalized fourth derivative of the slope  $\bar{i}_{\theta}$  method, which results from its better crack-recognition ability (as shown in Fig. 14), is applied in this research to crack identification of the

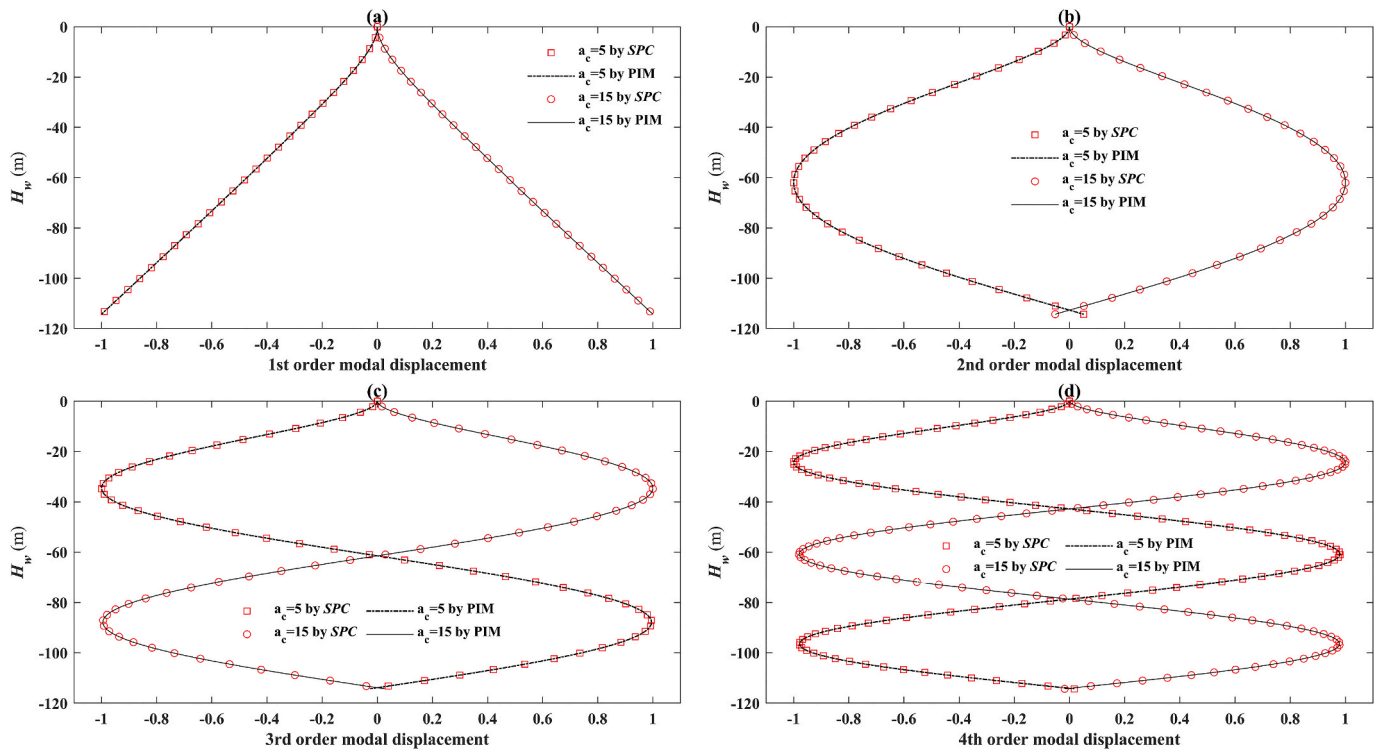


Fig. 8. First four modal shapes with 5- and 15-mm crack depths.

Table 5

First four natural frequencies of the cracked risers with different hang-off lengths.

	$n_k$	$\omega_1$	$\omega_2$	$\omega_3$	$\omega_4$
SPC <sub>i</sub>	5	0.31003585	2.57688477	5.59135535	9.44675492
	13	0.19014284	0.98478723	1.94169472	2.96529710
	22	0.14747018	0.61902017	1.18939554	1.78222238
	52	0.09872730	0.31537574	0.58130035	0.85764716
PIM <sub>i</sub>	5	0.31004547	2.57710420	5.59247783	9.45103857
	13	0.18966596	0.98454121	1.94239097	2.96431534
	22	Non	non	non	non
	52	Non	non	non	non

hang-off drilling riser during the deployment.

### 5.1. Based on the first-order modal results

The cracks are in the middle of the 15th, 26th, and 40th single riser joints with depths of 0.010, 0.015, and 0.020 m. In the final deployment, the riser joints, except for the upper two joints and lower three joints, are covered by the buoyancy blocks for convenience in the LMRP/BOPs installation and surface operations.

The crack identification using the first-order modal results in the deployment are shown in the supplementary video-data linked in Appendix A, where the first-order modal results of the 2nd, 8th, 20th, 30th, 45th, and 52nd steps of the installation are shown in Fig. 15.

The red bars in Fig. 15 indicate the crack indexes, and the Y and X coordinates of the captured data represent the locations and depths of the cracks, respectively. The linked video data indicate that the 1st, 2nd, and 3rd cracks appear at  $n_k = 17$ ,  $n_k = 28$ , and  $n_k = 42$ , respectively, which are larger than those of the pre-cracked single-riser numbers of 15, 26, and 40, respectively. The reason for the difference is that the data of the identification index  $\bar{t}_\theta$  are submerged in the data near the top riser joints, as shown in Fig. 15 and the video in Appendix A, which are further verified by comparison with the results presented in the next subsection.

### 5.2. Based on the higher modal results

For clear demonstration, the crack identifications using the 2nd, 3rd, and 4th modal results in the 20th and 52nd steps of the deployment are shown in Fig. 16.

Similarly, the red bars in Fig. 16 show the crack signals, and the Y and X coordinates of the captured data represent the crack locations and depths, respectively. The small value in the second crack in Fig. 16 (b) shows that the second modal results are not suitable for crack identification. By comparing Fig. 15 with Fig. 16, we can see that the identification index  $\bar{t}_\theta$  of the higher-order mode is more easily affected by the undesired data near both ends of the riser than that of the lower-order mode. However, the crack-identification index becomes more evident when the deployment continues, i.e., with the increase in  $n_k$ , as shown in Figs. 15 and 16.

### 5.3. The cracks at both ends

As presented in Sections 5.1 and 5.2, the cracks near both ends of the riser are challenging to be identified. The closer the crack is to both ends, the more difficult it is for them to be identified. Therefore, accurately detecting these cracks using index  $\bar{t}_\theta$  becomes the main objective of this study, as presented in this subsection.

A single crack is assumed to be located in the middle of the first single riser joint with a depth of 10 mm. When the first single joint is deployed, i.e.,  $n_k = 1$ , the results of the crack-identification index  $\bar{t}_\theta$  versus the discretized element numbers of 7, 11, and 21 are shown in Fig. 17 (a.1)–(a.3), respectively. When all the riser joints are deployed, i.e.,  $n_k = 52$ , the index  $\bar{t}_\theta$  of the top joint with the same element numbers of 7, 11, and 21 are shown in Fig. 17 (b.1)–(b.3), respectively. Similarly, the results of the bottom joint versus element numbers of 7, 11, and 21 are shown in Fig. 17 (c.1)–(c.3), respectively.

We need to note that the riser's vertical coordinates change from the value of the X coordinates in Fig. 17 (a) to that of X coordinates in Fig. 17 (c) from the start to the end of the installation. The results in Fig. 17(a–c) show that the crack is more easily identified at the end of the

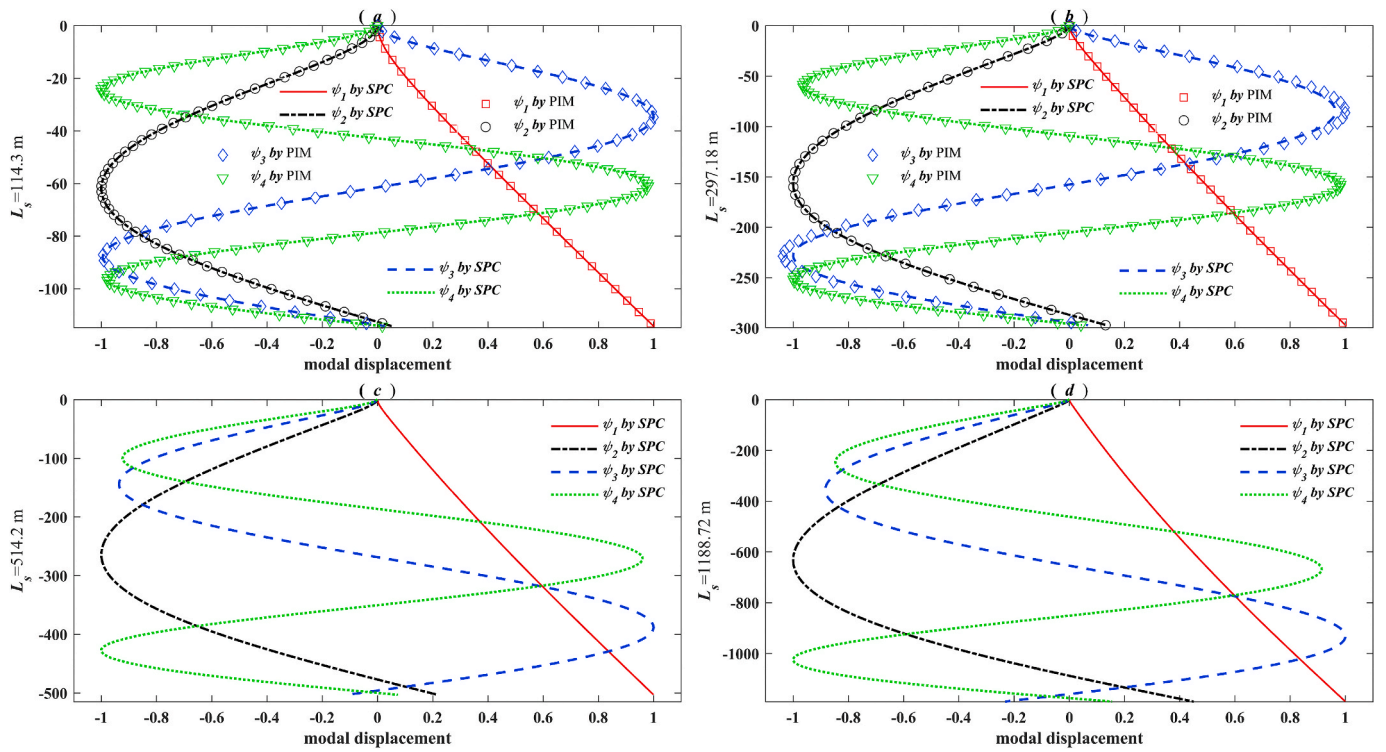


Fig. 9. First four modal shapes with different hang-off lengths.

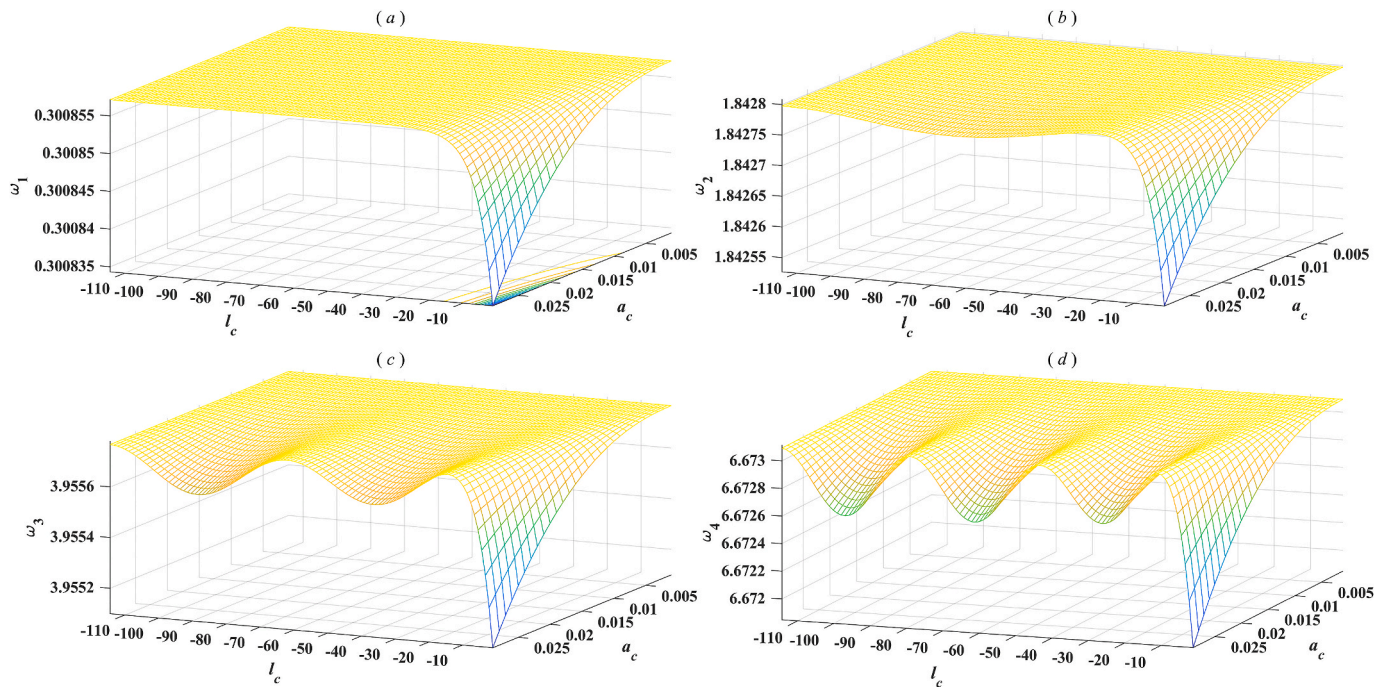


Fig. 10. First four natural frequencies of the short hang-off riser versus crack position and depth.

deployment process than at the start. Through comparison of Fig. 17 (a) and (b), we can see that the crack near the top end is more difficult to detect with the increase in the riser suspension length. Moreover, the sufficient number of discretized elements or the number of measurement points arranged in the engineering process contributes to the accuracy of the crack identification.

### 6. Conclusions

In this study, a numerical method for crack identification in a deepwater drilling riser was developed during its deployment. The correctness of programed code SPC was verified, and the performance of the modal-based approaches for crack identification was studied in detail. According to the results, the following few new and original conclusions were drawn.

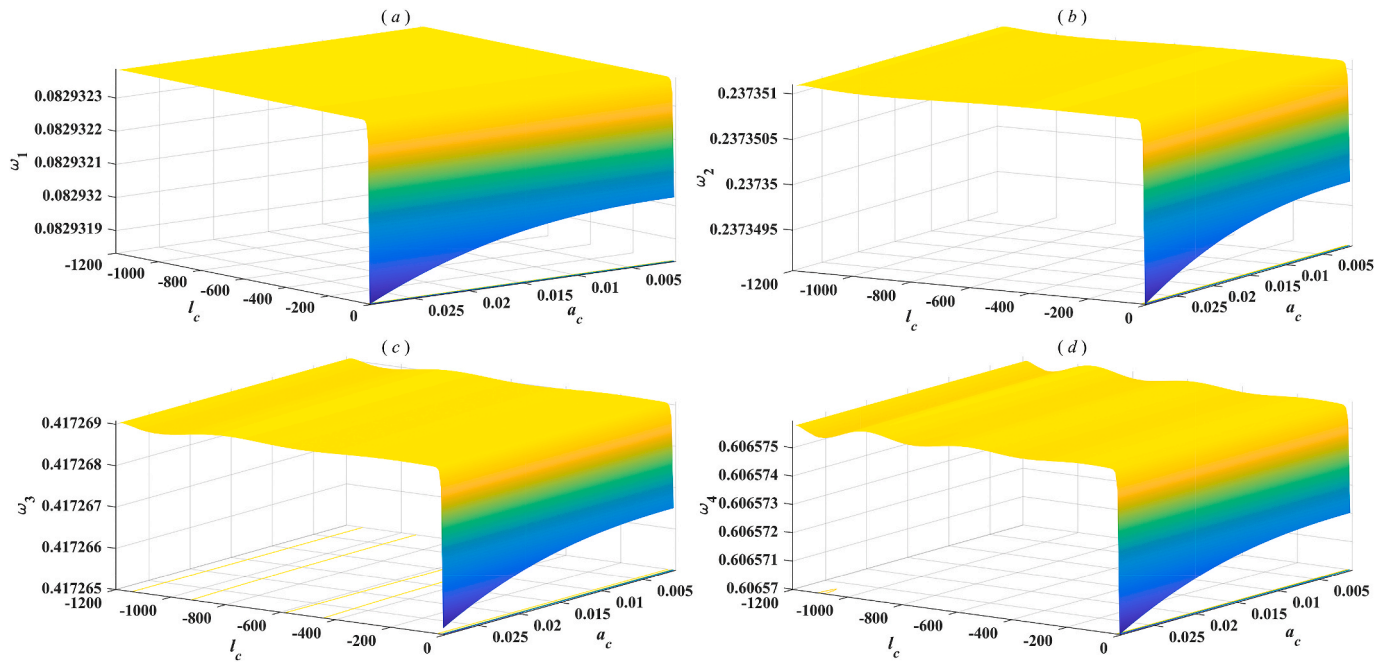


Fig. 11. First four natural frequencies of the long hang-off riser versus crack position and depth.

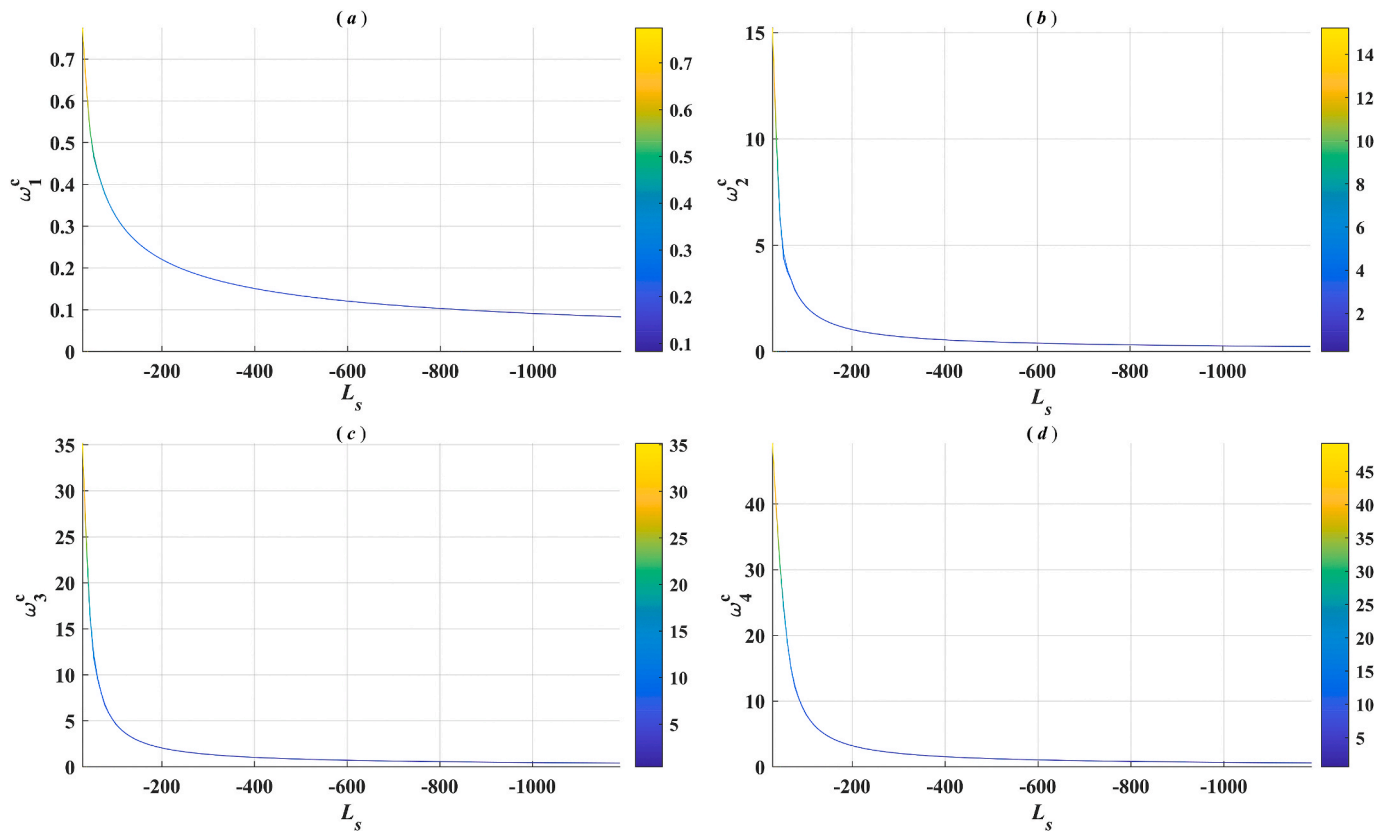


Fig. 12. Variation in first four natural frequencies versus  $L_s$  and  $a_c$ . Note: superscripts c represents the cracked natural frequency.

(1) The natural frequencies were significantly affected by the cracks that occurred near the top end. However, when the riser's suspension length was longer than approximately 200 m and the cracks were far from the top end, the natural frequencies were almost constant, regardless of the crack depths and positions.

(2) The frequency-based method for evaluating the open surface cracks of a deepwater drilling riser was limited, and the traditional modal curvature method for evaluating small cracks was limited unless intact riser information has already been known. Nevertheless, the normalized fourth derivative of the mode-slope

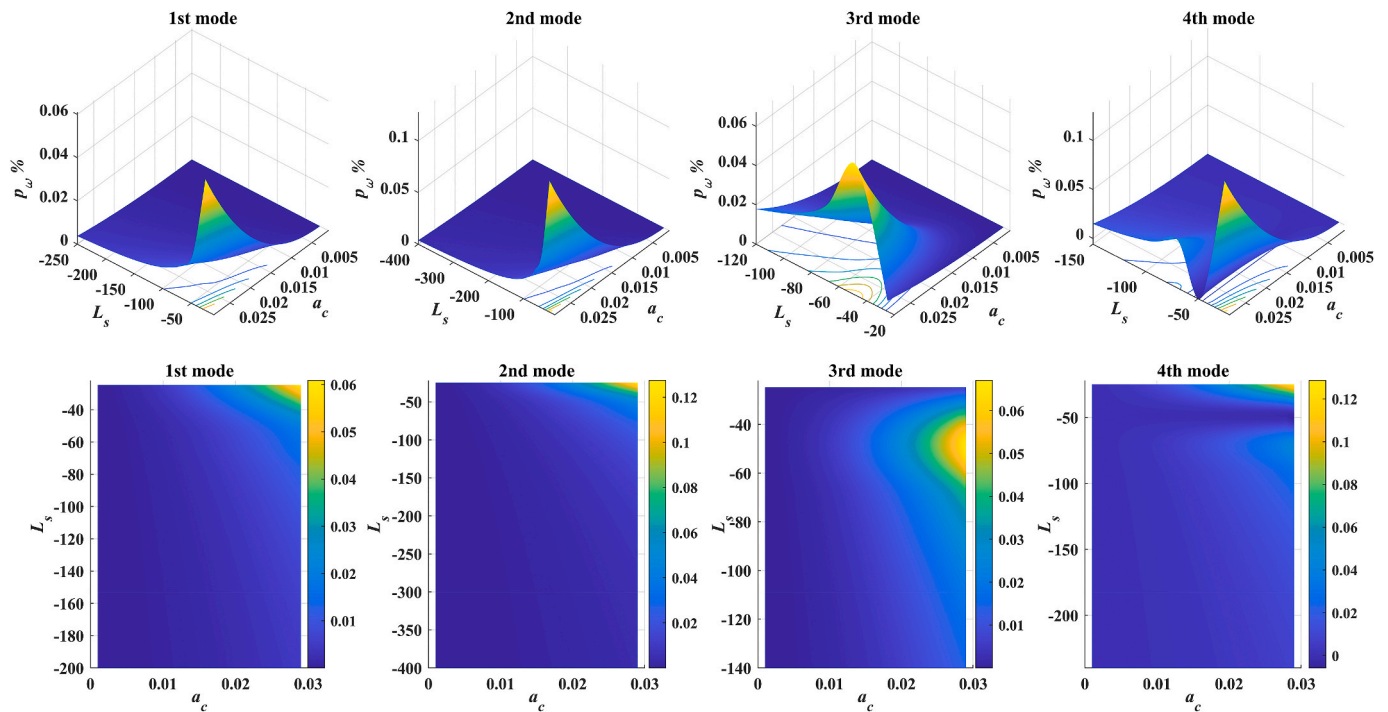


Fig. 13. Crack-detection possibility of  $\omega$  versus  $L_s$  and  $a_c$ .

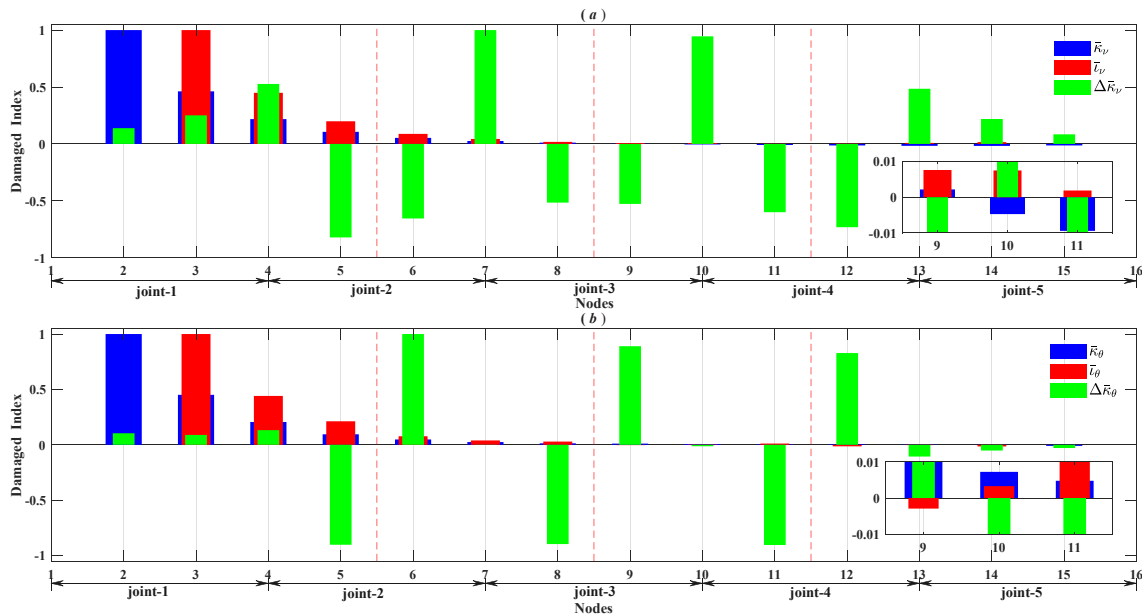


Fig. 14. Comparison of the different methods for crack identification.

method was sensitive to the surface open cracks without requiring the intact information.

- (3) The crack-identification index was easily affected by the undesired data near the top end, causing a hysteresis phenomenon in crack identification during the deployment. The higher the mode order was, the easier the crack-identification index was affected by the undesired data at both ends of the riser. Besides, crack identification became more relaxed and evident with the deployment continued.
- (4) In the deployment process, the previous cracked top joint became the current cracked bottom joint, and the crack was thus easily detected. However, a sufficient number of sensors were

recommended to be installed near the top riser joint to improve the crack-identification accuracy.

Above all, this study has provided a numerical method for crack identification of deepwater drilling risers with open surface cracks during the deployment. However, because of the assumption of coincidence of the crack nodes, cracks without thickness information would cause conservative calculation results. To more accurately simulate the actual cracks, a nonlinear equivalent cracked drilling-riser model that considers the effect of breathing or other types of cracks is suggested to be established in further research.

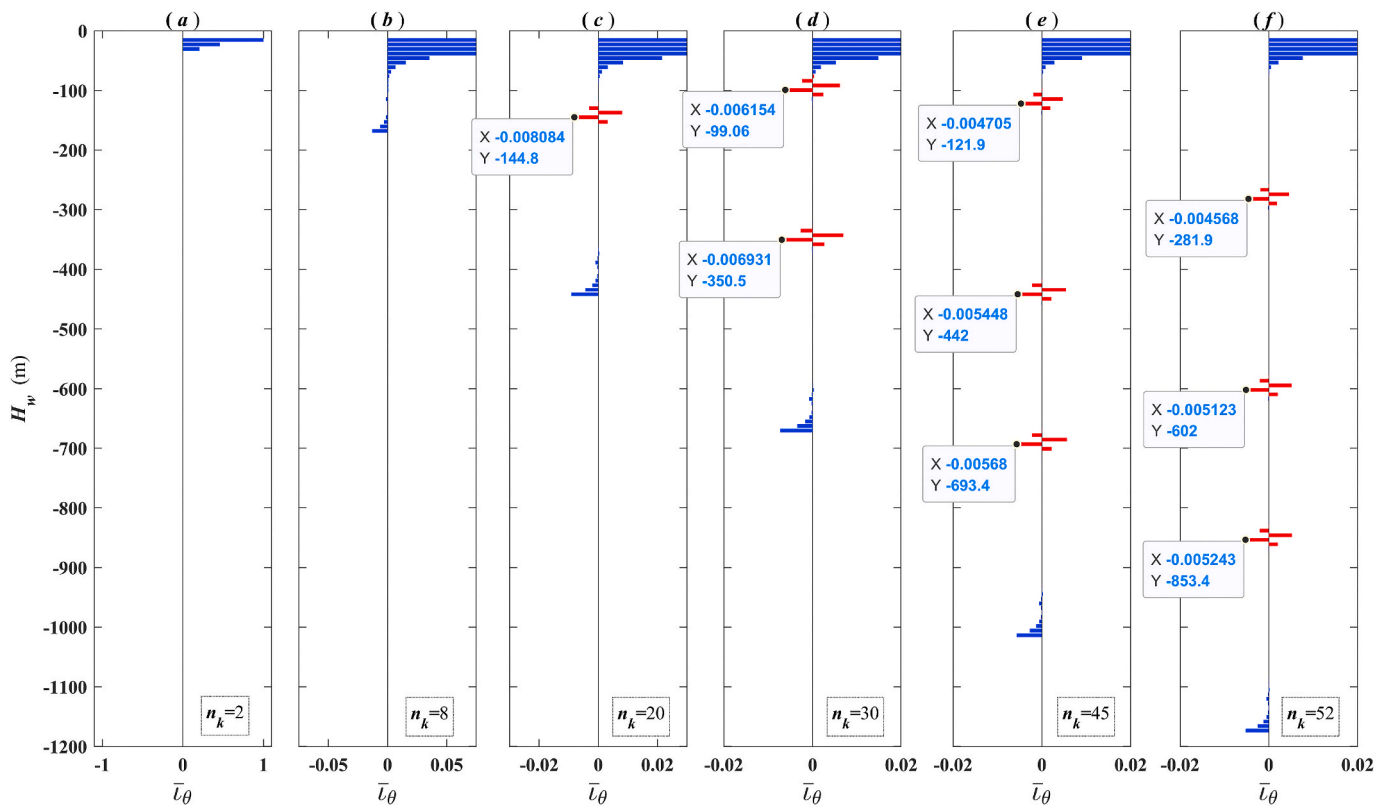


Fig. 15. Multiple-crack identification of first-order index  $\bar{\tau}_\theta$  during the deployment.

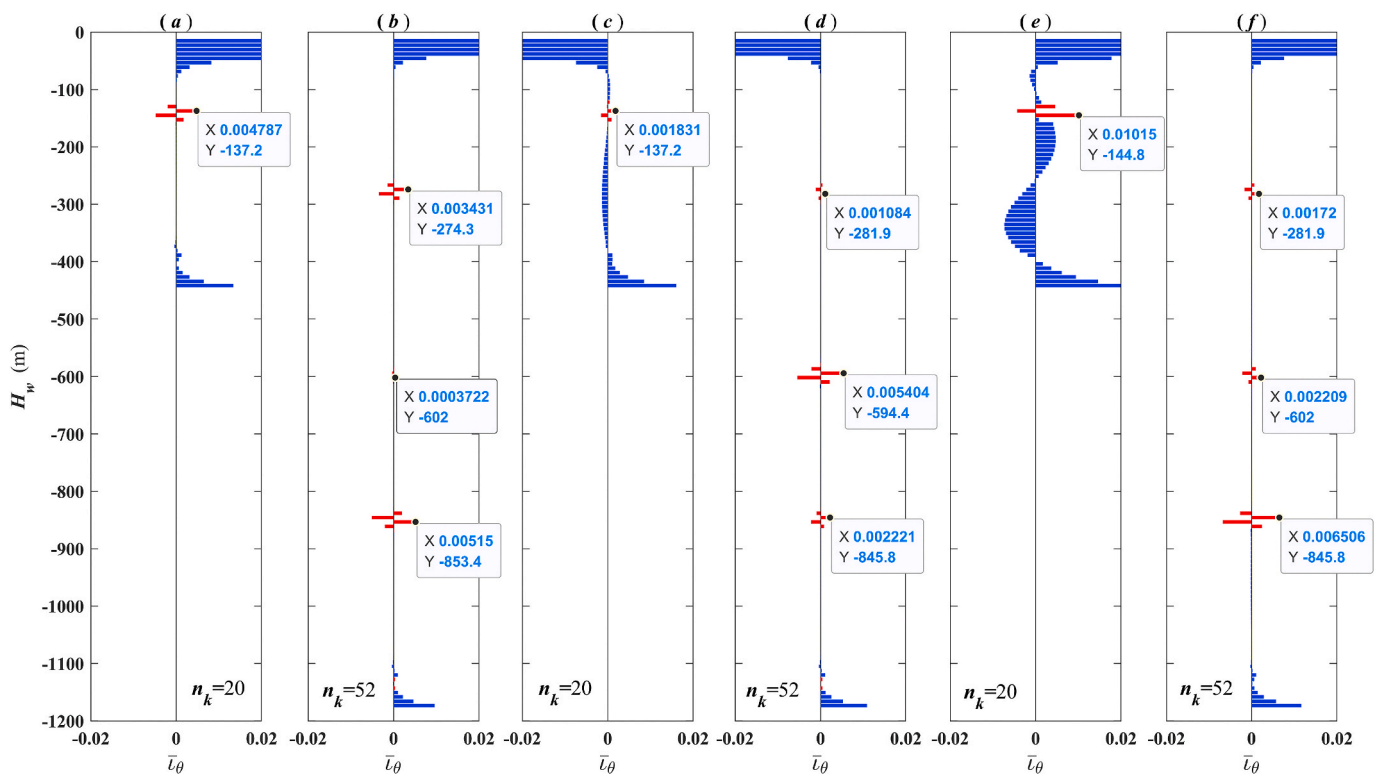


Fig. 16. Multiple crack identification of the higher order index  $\bar{\tau}_\theta$  during the deployment.

CRediT authorship contribution statement

Xingkun Zhou: Conceptualization, Methodology, Software,

Validation, Formal analysis, Investigation, Writing - original draft, Writing - review & editing. Yuqing Sun: Conceptualization, Methodology, Investigation, Writing - review & editing, Supervision, Resources,

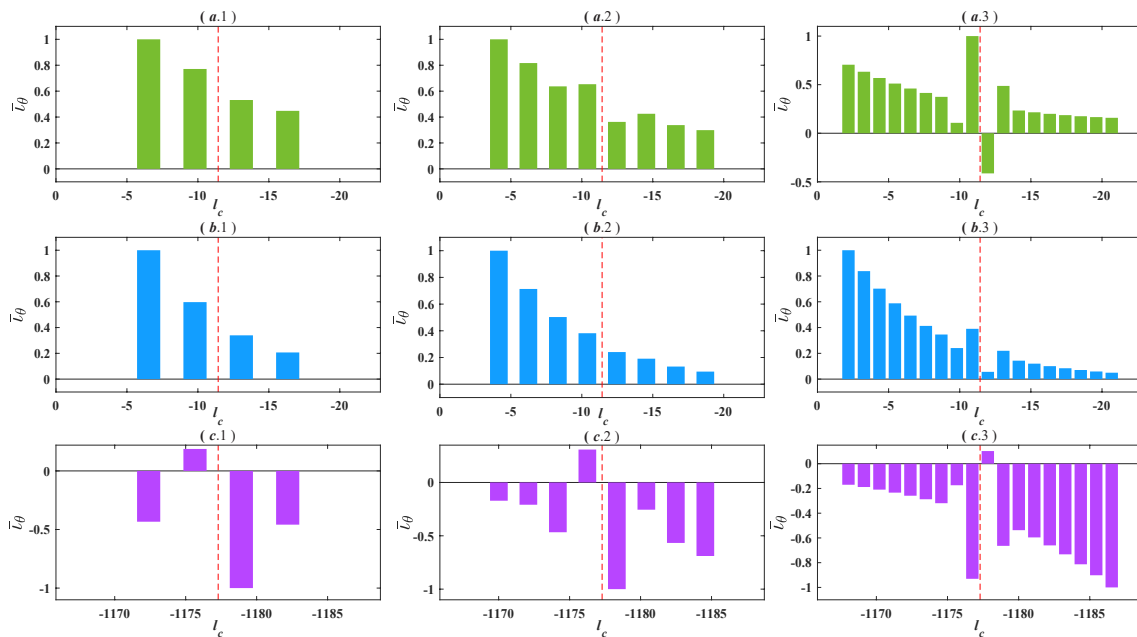


Fig. 17. Crack identification of the top and bottom joints at the beginning and end of the deployment. The red dashed lines show the pre-cracked positions. (For interpretation of the references to colour in this figure legend, the reader is referred to the Web version of this article.)

Project administration, Funding acquisition. **Menglan Duan:** Conceptualization, Methodology, Investigation, Validation, Formal analysis, Writing - review & editing. **Wenhua Li:** Conceptualization, Investigation, Validation, Resources, Project administration, Funding acquisition.

**Declaration of competing interest**

The authors declare that they have no known competing financial interests or personal relationships that could have appeared to influence the work reported in this paper.

**Acknowledgements**

The authors acknowledge the financial support from the “Fundamental Research Funds for Central Universities” with Grant No. 3132019041 and “the Funds for International Research Center of Subsea Technology and Equipment” with Grant No. 005448. We appreciate the contribution of professors Chen An and Yu Zhang at the China University of Petroleum-Beijing to the revision of the paper, and the kind comments and valuable suggestions from the reviewers and editors for improving the paper.

**Appendix A. Numerical model based on SP**

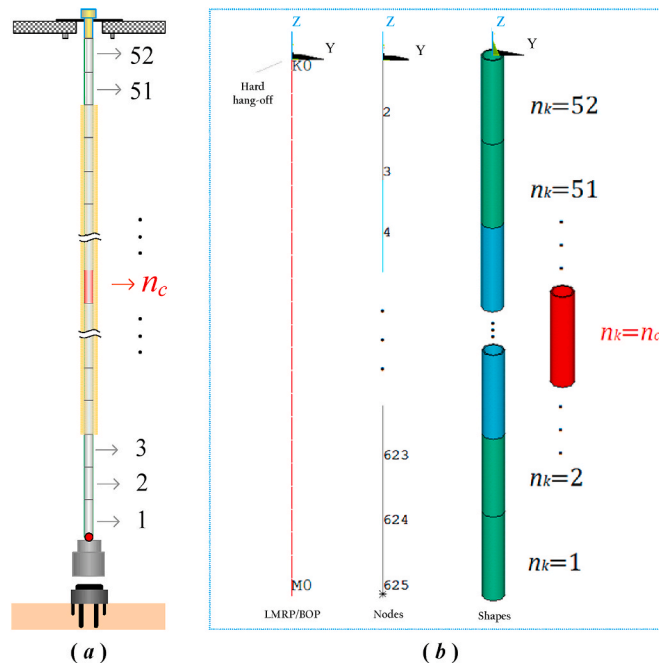


**Fig. B.** The established model based on the SPC code for crack identification during the deployment. (a) a crack-identification diagram, (b) a computational model using the SPC.

## Appendix B. Supplementary data

The crack identification in the deployment of a deepwater drilling-riser system is presented in the supplementary video file “Crack-identification based on the first-modal results.avi.”, which can be found online at: <https://doi.org/10.1016/j.petrol.2020.107721>.

## References

- American Bureau of Shipping (ABS), 2017. Guidance Notes on: Drilling Riser Analysis. Incorporated by Act of Legislature of the State of, New York.
- API-RP-14E, 2017. Recommended Practice for Design and Installation of Offshore Production Platform Piping Systems, fifth ed.
- API-RP-16Q, 2017. Design, Selection, Operation, and Maintenance of Marine Drilling Riser Systems, second ed.
- API-RP-2RD, 1998. Design of Risers for Floating Production Systems (FPSs) and Tension-Leg Platforms (TLPs), first ed.
- API-SPEC-5B, 2008. Specification for Threading, Gauging and Thread Inspection of Casing, Tubing, and Line Pipe Threads, fifteenth ed.
- Cummins, I., Todd, W., 2000. Deepwater Riser Management. SPE-59104-MS.
- Chen, Y., Chai, Y., Zhou, J., 2009. An extraction of the natural frequencies and mode shapes of marine risers by the method of differential transformation. *Comput. Struct.* 87 (21–22), 1384–1393.
- Chang, Y., Zhang, C., Wu, X., Shi, J., Chen, G., Ye, J., 2019. A bayesian network model for risk analysis of deepwater drilling riser fracture failure. *Ocean. Eng.* 181, 1–12.
- Dareing, D.W., Huang, T., 1979. Marine riser vibration response determined by modal analysis. *J. Energy Resour. Technol.* 101 (3), 159–166.
- DNV-RP-F204, 2010. Riser Fatigue.
- Drumond, G.P., Pasqualino, I.P., Pinheiro, B.C., Estefen, S.F., 2018. Pipelines, risers and umbilicals failures: a literature review. *Ocean. Eng.* 148 (15), 412–425.
- Fan, H., Wang, Z., Xu, L., Wang, Y., Feng, X., 2016. Dynamic analysis of a hang-off drilling riser considering internal solitary wave and vessel motion. *J. Nat. Gas Sci. Eng.* 37, 512–522.
- Fossum, T.O., 2013. Analysis and Control of Drilling Riser Dynamic in Dual Gradient Drilling. Norwegian University of Science and Technology ntnu-22358.
- Huang, C., Nagarajaiah, S., 2014. Output-only structural health monitoring for deepwater risers: experimental study of wavelet modified SOBI and distributed force index algorithm. *Int. J. Struct. Stabil. Dynam.* 14 (5), 1440010.
- Hariharan, M., Thethi, R., 2007. Drilling riser management in deepwater environments. New Delhi, India. In: The 7th International Oil & Gas Conference and Exhibition. January 15–19.
- He, Y., Ye, J., Chen, X., He, Z., 2009. Discussion on calculation of the local flexibility due to the crack in a pipe. *Mech. Syst. Signal Process.* 23 (3), 804–810.
- Jahangiri, M., Najafgholipour, M.A., Dehghan, S.M., Hadianfard, M.A., 2019. The efficiency of a novel identification method for structural damage assessment using the first vibration mode data. *J. Sound Vib.* 458, 1–16.
- Jacques, R., Clarke, T., Morikawa, S., Strohaecker, T., 2010. Monitoring the structural integrity of a flexible riser during dynamic loading with a combination of non-destructive testing methods. *NDT&E Int.* 43 (6), 501–506.
- Janeliukstis, R., Ručevskis, S., Kaewunruen, S., 2019. Mode shape curvature squares method for crack detection in railway prestressed concrete sleepers. *Eng. Fail. Anal.* 105, 386–401.
- Labib, A., Kennedy, D., Featherston, C., 2014. Free vibration analysis of beams and frames with multiple cracks for damage detection. *J. Sound Vib.* 333 (20), 4991–5003.
- Liu, H., Yang, H., Liu, F., 2014. Damage localization of marine risers using time series of vibration signals. *J. Ocean Univ. China* 13 (5), 777–781.
- Lozev, M.G., Smith, R.W., Grimmett, B.B., 2003. Evaluation of Methods for Detecting and Monitoring of Corrosion Damage in Risers, pp. OMAE2003-37350.
- Lei, S., Zhang, X., Kennedy, D., 2017. Dynamic response of a deepwater riser subjected to combined axial and transverse excitation by the nonlinear coupled model. *Int. J. Non Lin. Mech.* 97, 68–77.
- Min, C.H., Hong, S., Kim, H.W., Choi, J.S., Yeu, T.K., 2013. Structural health monitoring for top-tensioned riser with response data of damaged model. ISOPE-M-13-058.
- Mao, L., Zeng, S., Liu, Q., 2019. Dynamic mechanical behavior analysis of deep water drilling riser under hard hang-off evacuation conditions. *Ocean. Eng.* 183, 318–331.
- Moradi, S., Razi, P., Fatahi, L., 2011. On the application of bees algorithm to the problem of crack detection of beam-type structures. *Comput. Struct.* 89 (23–24), 2169–2175.
- Neidhardt, D., Ziegler, R.F., Lancaster, J., 2017. Drilling Riser Integrity Assurance for Deepwater Floating Drilling. OTC-27945-PT.
- Peter, J.D., Robinson, R., Metcalfe, T.J., Storesund, W., 2005. Fatigue Evaluation of Drilling Risers for Harsh Environments and Ultra Deepwater Developments to Allow Optimised Riser Life and Inspection Plans. SPE/ADC-92696.
- Sheng, L., Xu, L., Zhou, J., Jiang, S., Li, X., 2016. Experience on Deepwater Drilling Riser about Hang-Off Modes in Typhoon Condition of South China Sea. OTC-26616-MS.
- Tada, N., Uchida, M., 2012. Electric field analysis of simultaneous evaluation of crack on an inner pipe surface and pipe wall thickness using direct-current potential difference method of multiple-probe type. *J. Press. Vess.-T. ASME* 134 (41501), 1–10.
- Tian, D., Fan, H., Leira, B.J., Sævik, S., 2019. Study on the static behavior of installing a deep-water drilling riser on a production platform. *J. Petrol. Sci. Eng.* 185, 106652.
- Wang, Y., Gao, D., Fang, J., 2015. Mechanical behavior analysis for the determination of riser installation window in offshore drilling. *J. Nat. Gas Sci. Eng.* 34, 317–323.
- Yashar, A., Ferguson, N., Ghandchi-Tehrani, M., 2018. Simplified modelling and analysis of a rotating Euler-Bernoulli beam with a single cracked edge. *J. Sound Vib.* 420, 346–356.
- Ye, J., He, Y., Chen, X., Zhai, Z., Wang, Y., He, Z., 2010. Pipe crack identification based on finite element method of second generation wavelets. *Mech. Syst. Signal Process.* 24 (2), 379–393.
- Yu, D., Zou, L., Wan, D., 2017. Numerical analysis of multi-modal vibrations of a vertical riser in step currents. *Ocean. Eng.* 152, 428–442.
- Zheng, D., Fan, S., 2003. Vibration and stability of cracked hollow-sectional beams. *J. Sound Vib.* 267 (4), 933–954.
- Zhou, X., Duan, M., Jurado, G.J., 2018. Precise integration method for natural frequencies and mode shapes of ocean risers with elastic boundary conditions. *Appl. Math. Model.* 61, 709–725.
- Zhou, X., Wang, D., Duan, M., Gu, J., Liu, Y., 2017. Numerical study on mode curvature for damage detection of a drilling riser using transfer matrix technique, 2017 *Appl. Ocean Res.* 63, 65–75.